Resonances and thresholds in the Rydberg-level population of multiply charged ions at solid surfaces

Lj. D. Nedeljković and N. N. Nedeljković
Faculty of Physics, University of Belgrade, P.O. Box 368, 11001 Belgrade, Yugoslavia
(Received 3 April 1998; revised manuscript received 11 June 1998)

We present a theoretical study of resonances and thresholds, two specific features of Rydberg-state formation of multiply charged ions ($Z=6$, 7, and 8) escaping a solid surface at intermediate velocities ($v\approx 1$ a.u.) in the normal emergence geometry. The resonances are recognized in pronounced maxima of the experimentally observed population curves of Ar VIII ions for resonant values of the principal quantum number $n=n_{\rm res}=11$ and for the angular momentum quantum numbers $l=1$ and 2. Absence of optical signals in detectors of beam-foil experiments for $n>n_{\rm thr}$ of S VI and Cl VII ions (with $l=0$, 1, and 2) and Ar VIII for $l=0$ is interpreted as a threshold phenomenon. An interplay between resonance and threshold effects is established within the framework of quantum dynamics of the low angular momentum Rydberg-state formation, based on a generalization of Demkov-Ostrovskii's charge-exchange model. In the model proposed, the Ar VIII resonances appear as a consequence of electron tunneling in the very vicinity of the ion-surface potential barrier top and at some critical ion-surface distances R_c. The observed thresholds are explained by means of a decay mechanism of ionic Rydberg states formed dominantly above the Fermi level E_F of a solid conduction band. The theoretically predicted resonant and threshold values, $n_{\rm res}$ and $n_{\rm thr}$ of the principal quantum number n, as well as the obtained population probabilities $P_{nl}=P_{nl}(v,Z)$, are in sufficiently good agreement with all available experimental findings. [S0163-1829(98)05947-5]

I. INTRODUCTION

It has been known for a relatively long time that some multiply charged ions (e.g., with core charge $Z=6,7,8$) escaping solid surfaces in the normal emergence geometry capture a solid electron into a highly excited Rydberg state. Several papers[1–4] report that in the case of the hydrogenlike sulfur, chlorine, and argon (S VI, Cl VII, and Ar VIII) moving at intermediate velocities ($v\approx 1$ a.u.), a remarkable selective population of few Rydberg states around the principal quantum number $n\approx Z$ appears for all relevant angular momentum quantum numbers $l=0,1,\ldots,n-1$. In the cited beam-foil experiments, carbon foils have been used. The relative level population probabilities have been measured exclusively by methods of optical spectroscopy, detecting the photon deexcitations of formed Rydberg states in the outgoing part of the ionic trajectory. In the presentation of experimentally obtained population curves, an absence of an optical signal in the detector has been interpreted[4] as a vanishing population probability of the tested Rydberg states (n,l).

From a theoretical point of view, even in the simplest (normal emergence) geometry, the electron-capture processes into Rydberg states of a moving multiply charged ion represent an extremely complex quantum-mechanical problem. The quantum picture of the process essentially depends not only on the value of the ionic charge Z, but also on the velocity region of the ionic projectile. Over the past decade, many valuable contributions have been made to the *ab initio* quantum-mechanical calculations of relevant physical quantities as matrix elements and transition rates (see, for example, Refs. 5–8). Most of the theoretical studies performed so far have concentrated on the low velocity region ($v\ll 1$ a.u.) of the multiply charged ions, in which a resonant character of the electron-capture process is dominant. It is natural to expect, however, that with an increasing velocity v of the projectiles, both the adiabatic approximation and the supposition about resonant electron captures break down. Having faced the complexity of reported experimental data[1–4] we concluded that the selective population of Rydberg states $n\approx Z$ for $v\sim 1$ a.u. and $Z=6$, 7, and 8 must be considered from the very beginning as a nonadiabatic and nonresonant electron-capture process.

A systematic quantum-mechanical study of the cited experiments[1–4] has been developed recently,[9] under the restriction to the low angular momentum quantum numbers ($l=0$, 1, and 2). The mathematical basis for our dynamic quantum model has been found through a generalization of Demkov-Ostrovskii's asymptotic theory[10,11] (used previously in the study of ion-atom collisions at arbitrary velocities). The obtained formula for the population probability $P_{nl}(v,Z)$ of the Rydberg state (n,l) predicted very well the selectivity $n\approx Z$ of the electron-capture process as a basic experimental result in the intermediate velocity region of the multiply charged ionic projectile.

An important experimental fact, however, has not been supported by the cited model.[9] Namely, in the case of ionic Rydberg sublevels $l=1$ and 2 of Ar VIII, it has been observed[2] that the peak in the n dependence of $P_{nl}(v,Z)$ is shifted from the ''normal'' position $n\approx Z=8$ to $n=11$, becoming at the same time very pronounced [see Figs. 7(b) and 7(c)]. In other words, a resonance-type shape has been evidently superimposed on the ''normal'' forms of the population curves, suggesting a kind of resonance phenomenon.

There was also an additional detail in some of the experimentally registered population curves which has not been taken into account more carefully in our model.[9] Namely, in

the case[3,4] of the ions S VI and Cl VII with $l=0$, 1, and 2, as well as in the case[2] of the Ar VIII ion with $l=0$, the experimentally observed P_{nl} curves rapidly decrease after their ''normal'' maxima at $n\approx Z$ [see Figs. 5, 6, and 7(a)], whereas the proposed model[9] predicts a slightly slower decreasing of the curves. In other words, instead of the resonance forms of Ar VIII type (with $l=1$ and 2), the shapes of the experimentally obtained population curves for these cases suggest a thresholdlike behavior in the higher n region. It is worth noting that a dilemma about the interpretation of the population curves for higher n values has been present from the very beginning of the experimental studies of the Rydberg-state formation at solid surfaces (see, for example, Refs. 12 and 4).

This paper is devoted to an analysis of the resonance and threshold phenomena in the context of further elaboration of our quantum nonresonant dynamic model.[9] We realized that the study of these phenomena requires a few nontrivial mathematical extensions of the asymptotic methodology exposed in Ref. 9. In the framework of the energy eigenproblem calculations (fixed ion-surface distance R) it was necessary to find a new set of the energy eigenfunctions valid in the very vicinity of the ion-surface potential barrier top. In that sense, a generalization of Slavyanov's etalon equation method[13,14] has been done (instead of the JWKB method[9]). The previously used[9] electron-capture quantum dynamics ($R=vt \neq \text{const}$) of Demkov-Ostrovskii's type is extended by the method of the complex eigenenergies.[15] This has been done in order to include an ionization mechanism activity appearing with those ionic Rydberg states dominantly populated above the Fermi level E_F of the solid conduction band. Our ϱ-matrix multichannel approach[9] to the final expression for the population probability $P_{nl}(v,Z)$ is elaborated in accordance with the changes cited above.

The following physical picture of the Rydberg-level population of multiply charged ions at solid surfaces emerges from the analysis which will be explicated in this paper. First of all, from the standpoint of a pure electron-capture process, the ''resonances'' (defined as the ionic Rydberg states with $n=n_{\text{res}}$ and populated with sufficiently high probabilities) are not characteristic only of the Ar VIII ions but also the ions of S VI and Cl VII. However, in the case of S VI and Cl VII ions for $l=0$, 1, and 2 as well as for $l=0$ of Ar VIII, these Rydberg resonances are formed dominantly at some critical ion-surface distance $R_c=R_c(n,l,Z,v)$ when their energy levels E_A are positioned above the Fermi level E_F of the solid. Accordingly, they will be destroyed fast by the resonant ionization mechanism. Such kinds of short-lived Rydberg resonances will not be able to send a sufficiently intense photon radiation before their ionization decay; in that sense we can say that they will be ''hidden'' from the standpoint of the detection system of optical spectroscopy. The same holds for all other Rydberg states (n,l) formed by the electron capture above E_F, i.e., for levels satisfying the condition $n>n_{\text{thr}}$. Thus, the absence of the signals in the detector appears as a thresholdlike behavior of P_{nl} curves. Our calculations of threshold values n_{thr} are in a sufficiently good correlation with experimental data (see Figs. 5, 6, and 7).

On the other hand, the Rydberg resonances of Ar VIII ions for $l=1$ and 2 are formed below the Fermi level E_F so that the ionization of these states will be suppressed by the filled valence band of the solid. Their photon deexcitations will result in very pronounced and experimentally observable peaks in P_{nl} curves. Roughly speaking, the Ar VIII resonances (with $l=1$ and 2) are formed dominantly at critical ion-surface distances R_c by an electron tunneling in the very vicinity of the potential barrier top. In other words, the high values of P_{nl} for $n=n_{\text{res}}$ of the mentioned Ar VIII cases can be attributed to a high transparency of the ion-surface barrier under the described conditions. Our calculations showed that the resonant values n_{res} are placed just at the experimentally detected value $n_{\text{res}}=11$ [see Figs. 7(b) and 7(c)]. Moreover, the shapes of the theoretically predicted P_{nl} graphs around $n=n_{\text{res}}$ coincide well with the experimental findings.

This paper is organized as follows. In Sec. II we formulate the problem in the context of our model of the Rydberg-state population process. Section III is devoted to the study of the energy eigenproblem of the ion-surface system. Quantum dynamics of the process is treated in Sec. IV, in which we calculated the experimentally verifiable population probability P_{nl}. Some relevant concluding remarks will be given in Sec. V.

Atomic units ($e^2=\hbar=m_e=1$) will be used through the paper unless indicated otherwise.

II. FORMULATION OF THE PROBLEM

A general structure of our model of the Rydberg-state formation at a solid surface has been described previously.[9] In this section we shall formulate the problem, explicating in more detail only those points which are relevant in our subsequent discussions.

A. Eigenproblem of the Hamiltonian

We consider an active electron (e^-) of the process in the Coulomb field of pointlike multiply charged ionic core ($Z \gg 1$) and in the field of a polarized semi-infinite conducting solid. For fixed and large R, the polarized solid interacts with the electron e^- (positioned outside the solid) by forces of the electron image (e^+) and of the ionic core image ($-Z$); Fig. 1(a). The potential of the active electron placed inside the solid is described by the Sommerfeld model. Difficulties with forms of the image potentials in the near surface region will not be essential[11] in determination of the population probability within the asymptotic methodology applied in this paper. Behavior of the total potential U of the active electron along the z axis is presented in Fig. 1(b).

In our subsequent discussion, two types[9] of molecularlike eigenfunctions of the Hamiltonian H of the active electron will play an important role, corresponding to the continuous and discrete parts of the energy spectrum. We have

$$H\Phi_{MA}=E\Phi_{MA}, \quad E=-\frac{\gamma^2}{2} \tag{2.1a}$$

and

$$H\Phi_{AM}=E_A\Phi_{AM}, \quad E_A=-\frac{\gamma_A^2}{2}, \tag{2.1b}$$

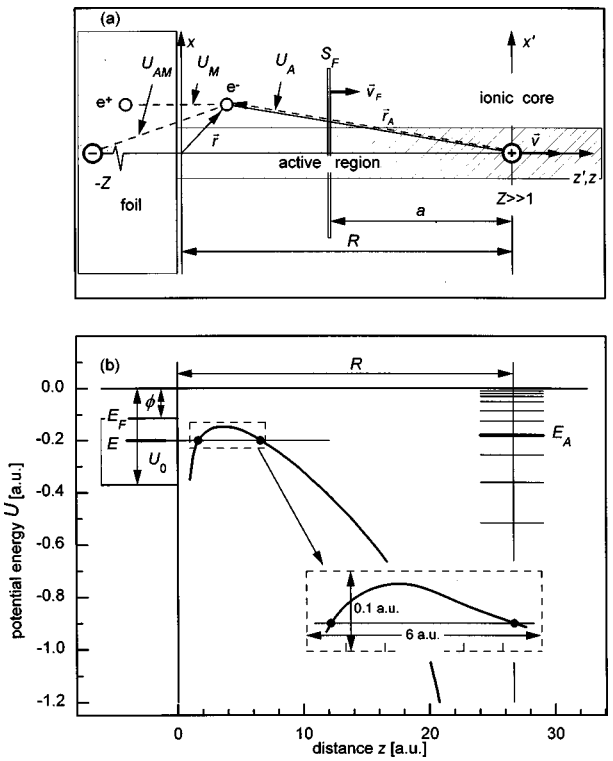

FIG. 1. (a) Geometry of the process. The potentials U_A, U_M, and U_{AM} are explicated in Ref. 9. (b) Energies of the process in the stage when the electron-capture probability reaches maximum [Ar VIII ion at ion-surface distance $R_c=26.6$ a.u., $E=-\gamma/2$, $\gamma=0.6$ a.u.; the parameters R_c and γ correspond to the electron capture into the Rydberg state ($n=10$, $l=1$)]. Note a relatively flat plate of the potential curve $U=U_A+U_M+U_{AM}$.

where γ and γ_A are the corresponding continuous and discrete energy parameters, respectively.

The energy eigenproblem (2.1a) for the function Φ_{MA} will be solved in the narrow cylindrical region around the z axis [see Fig. 1(a)] representing the most relevant region for the electron transitions into the low angular momentum Rydberg states $l=0$, 1, and 2. In that case we can separate variables in the eigenproblem (2.1a) by using the parabolic coordinates $\xi=r_A+z_A$, $\eta=r_A-z_A$, and $\varphi=\arctan(y/x)$.

We express the function Φ_{MA} in the form

$$\Phi_{MA}=\frac{X_{MA}(\xi)Y_{MA}(\eta)}{\sqrt{\xi\eta}}\exp(\pm im\varphi), \tag{2.2}$$

where

$$\frac{d^2X_{MA}(\xi)}{d\xi^2}+P^2(\xi,\beta_1)X_{MA}(\xi)=0, \tag{2.3a}$$

$$\frac{d^2Y_{MA}(\eta)}{d\eta^2}+Q^2(\eta,\beta_2)Y_{MA}(\eta)=0, \tag{2.3b}$$

whereas m stands for the absolute value of the magnetic quantum number ($m=0,1,2,\ldots$). The relevant separation constants β_1 and β_2 are related by $\beta_1+\beta_2=Z$. We impose the following boundary conditions: $X_{MA}(0)=0$, $X_{MA}(\infty)=0$ and $Y_{MA}(0)=0$, $Y_{MA}(\eta)=$(incoming+reflecting wave), in solid.

The variables of the eigenproblem (2.1b) can be separated in two different ways, depending on the relevant space regions. Restricting ourselves to the large region around the ionic core [see Fig. 1(b)], a separation of variables in spherical coordinates is possible, so that we have the eigenfunction $\Phi_{AM}=\Phi_{AM}(r,\theta,\varphi)$ associated with the quantum numbers (n,l,m_A). On the other hand, in the bulk of the solid and in the region around the ionic core, as well as in the narrow cylindrical region around the z axis, the separation of variables is possible by using the parabolic coordinates, which leads us to the function $\Phi_{AM}=\Phi_{AM}(\xi,\eta,\varphi)$ characterized by the parabolic quantum numbers (n_{1A},n_{2A},m_A).

For the purpose of quantum dynamics we need exclusively those parabolic states $\Phi_{AM}(\xi,\eta,\varphi)$ associated with the energy levels E_A above the Fermi level E_F so that the boundary conditions are given by $X_{AM}(0)=0$,$X_{AM}(\infty)=0$ and $Y_{AM}(0)=0$,$Y_{AM}(\eta)=$ outgoing wave, in solid. The latter of the two conditions indicates that the metallic states above the Fermi level E_F are empty (in the cold metal approximation) and can be occupied by a time-decay mechanism of the eigenstate $\Phi_{AM}(\xi,\eta,\varphi)$. The corresponding ionization rate $\Gamma_\mu^{\rm ion}(R)$ is defined by[15]

$$\breve{E}_A(R)=E_A(R)-\frac{i}{2}\Gamma_\mu^{\rm ion}(R), \tag{2.4}$$

where $\breve{E}_A(R)$ represents the complex energy of the eigenproblem (2.1b) for fixed and large R. The index μ stands for a set of parabolic quantum numbers associated with the function Φ_{AM}.

B. Quantum dynamics of the Rydberg-state formation

We shall first formulate the electron-capture dynamics neglecting the possibility of the Rydberg-state ionization. After that we pass to a more realistic, ''renormalized'' quantum dynamics, which takes into account the ionization mechanism of Rydberg states dominantly formed above E_F.

We consider the electron capture into the Rydberg state (n,l) as an electron transition from its solid eigenstate Φ_M^γ (at time $t=0$) to a moving atomic state $\varphi_A^{nl}(t)$. A procedure explicated in Ref. 11 (briefly reviewed in Ref. 9) enables us to express the transition probability of the process in terms of the mixed electron flux $I(t)$ through a moving Firsov plane S_F, positioned between the solid surface and the moving ion [see Fig. 1(a)]. Namely, we have

$$I(t)=\frac{i}{2}\int_{S_F}\left[\frac{\nabla\Psi_M^\gamma}{\Psi_M^\gamma}-\frac{\nabla\Psi_A^{nl*}}{\Psi_A^{nl*}}-2iv\left(1-\frac{da}{dR}\right)\mathbf{e}_z\right]\Psi_A^{nl*}\Psi_M^\gamma d\mathbf{S}, \tag{2.5}$$

where $a=a(t)$ denotes the S_F plane instant position with respect to the moving ion, whereas $d\mathbf{S}=dS\mathbf{e}_z$. The time-dependent wave function $\Psi_M^\gamma(t)$ represents an evolved initial state $\Phi_M^\gamma(\mathbf{r})$ at time t. For Ψ_A^{nl} we have a state that will evolve into the moving atomic state $\varphi_A^{nl}(t)$ at $t\to\infty$. At sufficiently large ion-surface distance $R=vt$, we take[9] that the functions $\Psi_M^\gamma(\mathbf{r},t)$ and $\Psi_A^{nl}(\mathbf{r},t)$ represent the space-time

modifications of the eigenstates Φ_{MA} and Φ_{AM} [Eqs. (3.13a) and (3.3) of Ref. 9, respectively].

The electron-capture transition probability from a set of initial states of unit γ interval (around given γ) of the foil valence band to the moving Rydberg state (n,l) during a finite time interval from $t=0$ to t is determined by[9]

$$T_{nl}^{\gamma}(t)=\left|\int_0^t I(t)dt\right|^2. \tag{2.6}$$

In order to estimate the critical ion-surface distance R_c where the electron-capture process takes place dominantly, we use the normalized electron-capture rate

$$\tilde{\Gamma}_{nl}^{\gamma}(R)=\frac{1}{T_{nl}^{\gamma}}\frac{dT_{nl}^{\gamma}(t)}{dR}, \tag{2.7}$$

where $T_{nl}^{\gamma}=T_{nl}^{\gamma}(\infty)$. By definition, the critical distance R_c represents the position of maximum of the transition rate $\tilde{\Gamma}_{nl}^{\gamma}(R)$ as a function of R.

The ionization mechanism of the Rydberg states of the multiply charged ions escaping a solid surface at intermediate velocities is not yet known in more detail. It is a separate and complex problem to incorporate simultaneously the ionization and electron capture from the very beginning of the calculation in a dynamic model of Demkov-Ostrovskii's type. We realized that a sufficiently good approach, correlating with the existing experimental facts,[2–4] can be based on the following transformation of the function $\Psi_A^{nl}(t)$:

$$\Psi_A^{nl}(t)\rightarrow\overline{\Psi}_A^{nl}(t)=\mathcal{E}_{\mu_0}(t)\Psi_A^{nl}(t), \tag{2.8}$$

where

$$\mathcal{E}_{\mu_0}(t)=\exp\left[-\frac{1}{2}\int_0^t\Gamma_{\mu_0}^{\mathrm{ion}}(R)dt\right]\ll 1, \tag{2.9}$$

whereas μ_0 represents a set of parabolic quantum numbers corresponding to the leading state from a set of all possible intermediate states $\Phi_{AM}=\Phi_{AM}(\xi,\eta,\varphi)$.

By using the fast ionization condition (2.9) we can obtain a transformed expression for the transition probability T_{nl}^{γ} into a Rydberg state (n,l) dominantly formed above E_F, i.e., for $R_c<R_F$. The ion-surface distance R_F is defined by $|E_A(R_F)|=\phi$, where ϕ denotes the work function of the solid. On the other hand, the influence of the ionization process on the electron transitions localized mainly at $R_c>R_F$ is negligible. Therefore, including the ionization, we arrive to the following expression for T_{nl}^{γ}:

$$T_{nl}^{\gamma}=\left|\int_0^{\infty}I_{nl}^{\gamma}(t)dt\right|^2;\quad R_c>R_F, \tag{2.10a}$$

$$T_{nl}^{\gamma}=\left|\int_{R_F}^{\infty}I_{nl}^{\gamma}(t)dt\right|^2;\quad R_c\leqslant R_F. \tag{2.10b}$$

We specified the initial and final states in the mixed flux $I(t)$ by using the notation $I(t)=I_{nl}^{\gamma}(t)$.

The population probability P_{nl} of a Rydberg state (n,l) is given by the multichannel expression[9]

$$P_{nl}=[1-\exp(-T_{nl})]\exp\left(-\sum_{n'\neq n}\langle T_{n'l'}\rangle_{l'}\right), \tag{2.11}$$

where $T_{nl}=\int\Sigma n_{\gamma}T_{nl}^{\gamma}d\gamma$ is the total transition probability and $\langle T_{n'l'}\rangle_{l'}$ denotes the averaged value of the transition probability $T_{n'l'}$ with respect to l'.

III. CALCULATION OF THE ENERGY EIGENFUNCTIONS Φ_{MA} AND Φ_{AM}

Our first task is to calculate the parabolic eigenfunctions $\Phi_{MA}(\xi,\eta,\varphi)$, which will be done in Secs. III A, III B, and III C. The results obtained can be used in the study of the parabolic $\Phi_{AM}(\xi,\eta,\varphi)$ states (Sec. III D). At the end of Sec. III D we shall discuss the spherical eigenfunctions $\Phi_{AM}(r,\theta,\varphi)$.

A. Scaling procedure

Differential equations (2.3a) and (2.3b) can be transformed by an appropriate scaling procedure into the forms suitable for application of the etalon equation method.

In the scaling procedure of the X_{MA} equation we introduce the scaling parameter $\alpha_{\xi}=-4\tilde{E}R/(Z-1)$, where $\tilde{E}=E-\Delta E$ and $\Delta E=(2Z-1)/(4R)$, as well as the scaled variable $\tilde{\xi}=\xi/(2R\alpha_{\xi})$. Thus, we arrive at a scaled equation of the form (2.3a), but with the scaled quasimomentum

$$\tilde{P}^2(\tilde{\xi},\alpha_{\xi})=-b_{\xi}^2\frac{p_{\xi}^2(\tilde{\xi})}{4}+b_{\xi}\frac{\tilde{\lambda}_{\xi}}{\tilde{\xi}}+\frac{\tau}{\tilde{\xi}^2}, \tag{3.1a}$$

where

$$b_{\xi}=2R\alpha_{\xi}\sqrt{-2\tilde{E}},\quad \tilde{\lambda}_{\xi}=\frac{\beta_1}{\sqrt{-2\tilde{E}}},\quad \tau=\frac{1-m^2}{4}. \tag{3.1b}$$

The function $p_{\xi}(\tilde{\xi})$ is defined by

$$p_{\xi}^2=1+\frac{\tilde{\xi}}{1-\tilde{\xi}/\tilde{\xi}_0}, \tag{3.1c}$$

where $\tilde{\xi}_0=(2/\alpha_{\xi})(Z-1/2)/(Z-1)$.

Passing to a scaling procedure of the differential equation (2.3b) for the function $Y_{MA}(\eta)$, we introduce the second scaling parameter

$$\alpha\equiv\alpha_{\eta}=-\frac{2ER}{Z-\frac{1}{4}}, \tag{3.2a}$$

as well as the scaled variable $\tilde{\eta}=\eta/(2R\alpha)$. The corresponding scaled quasimomentum is given by

$$\tilde{Q}^2(\tilde{\eta},\alpha)=-b^2\frac{p^2(\tilde{\eta},\alpha)}{4}+b\frac{\tilde{\lambda}}{\tilde{\eta}}+\frac{\tau}{\tilde{\eta}^2}, \tag{3.2b}$$

where

$$b=2R\alpha\sqrt{-2E},\quad \tilde{\lambda}=\frac{\beta_2}{\sqrt{-2E}}. \tag{3.2c}$$

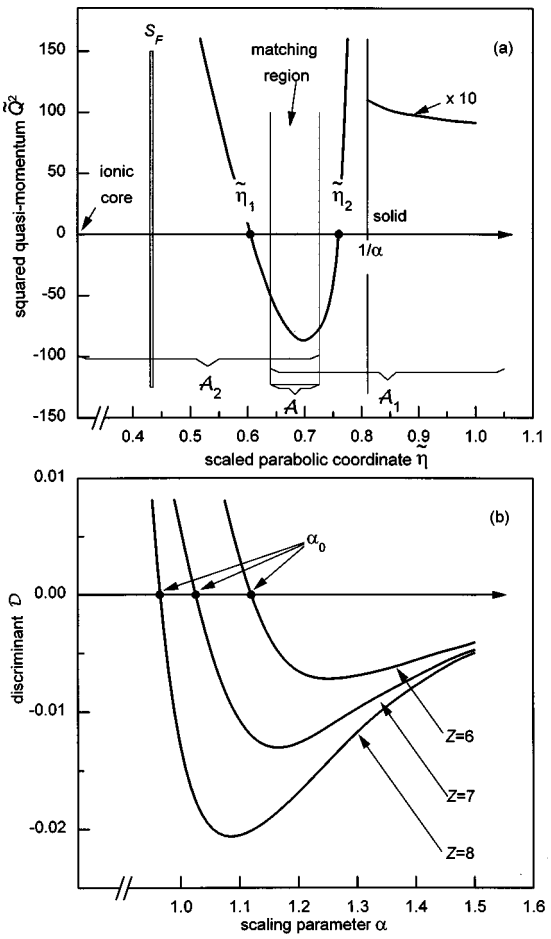

FIG. 2. (a) Typical behavior of the function $\tilde{Q}^2$ along the $\tilde{\eta}$ axis. (Parameters of the system are the same as in Fig. 1; for these parameters $\alpha=1.24$.) (b) The α dependence of $\mathcal{D}(\alpha,Z)$ for $Z=6$, 7, and 8.

The function $p^2(\tilde{\eta},\alpha)$ is defined by

$$p^2=1+\begin{cases}\dfrac{2}{\alpha}\dfrac{2-\alpha\tilde{\eta}_0}{2-\alpha\tilde{\eta}}-\dfrac{2}{\alpha}\dfrac{1-\alpha\tilde{\eta}_0}{1-\alpha\tilde{\eta}}; & \tilde{\eta}<1/\alpha\\ U_0/E; & \tilde{\eta}>1/\alpha,\end{cases} \tag{3.2d}$$

where $\tilde{\eta}_0=(1/\alpha)(Z-1/2)/(Z-1/4)$. For the function $p=p(\tilde{\eta})$ we adopted the following phase convention: $p=|p|$ for $p^2>0$ and $p=i|p|$ for $p^2<0$.

A typical behavior of the function $\tilde{Q}^2(\tilde{\eta},\alpha)$ is illustrated in Fig. 2(a) for fixed α, b, $\tilde{\lambda}$, and τ. The turning points $\tilde{\eta}_1$ and $\tilde{\eta}_2$ satisfy a third-order algebraic equation of the form $\tilde{\eta}^3+a_1\tilde{\eta}^2+a_2\tilde{\eta}+a_3=0$. Its coefficients are expressed exclusively in terms of α and Z; moreover, for sufficiently large Z, the α dependence is dominant.

A classification of the turning points configurations with respect to the values of α can be done by using the discriminant $\mathcal{D}=\mathcal{D}(\alpha,Z)$ of the mentioned algebraic equation. In Fig. 2(b) we presented the α dependence of the $\mathcal{D}(\alpha,Z)$ function for relevant values $Z=6$, 7, and 8 of the experimentally investigated ions S VI, Cl VII, and Ar VIII. In the limiting case $\tilde{\eta}_1=\tilde{\eta}_2$, the values of the scaling parameter α are determined by $\mathcal{D}(\alpha_0,Z)=0$. By solving this equation we obtain the values $\alpha_0=1.115$, 1.035, and 0.965 for $Z=6$, 7, and 8, respectively.

B. Application of the etalon equation method

The scaled differential equations for the functions $\tilde{X}_{MA}(\tilde{\xi})$ and $\tilde{Y}_{MA}(\tilde{\eta})$ will be solved by using a procedure based on Slavyanov's etalon equation method.[13,14] Its application to the $\tilde{X}_{MA}(\tilde{\xi})$ case follows the standard etalon equation treatment. However, a generalization of Slavyanov's method is necessary for solving the $\tilde{Y}_{MA}(\tilde{\eta})$ equation.

We look for a solution $\tilde{X}_{MA}(\tilde{\xi})$ regular at $\tilde{\xi}=0$ in the form

$$\tilde{X}_{MA}(\tilde{\xi})=\frac{1}{\sqrt{u'_\xi}}M_{\lambda_\xi,m/2}(b_\xi u_\xi), \tag{3.3}$$

where $M_{\lambda_\xi,m/2}(b_\xi u_\xi)$ represents the Whittaker function, whereas u_ξ is an etalonic variable and $u'_\xi=du_\xi(\tilde{\xi})/d\tilde{\xi}$. The scaled boundary condition $\tilde{X}_{MA}(\infty)=0$ will be satisfied only if

$$\lambda_\xi=n_1+\frac{m+1}{2}, \tag{3.4}$$

where $n_1=0,1,2,\ldots$ denotes the parabolic quantum number. In the lowest order of approximation we obtain $b_\xi u_\xi\approx\gamma\xi$ and $u'_\xi\approx1$, so that we can write

$$\tilde{X}_{MA}(\tilde{\xi})=X_{MA}(\xi)=M_{n_1+(m+1)/2,m/2}(\gamma\xi). \tag{3.5}$$

On the other hand, using the obtained value for the scaled spectral parameter $\tilde{\lambda}_\xi$, we have

$$\beta_1\approx\lambda_\xi\sqrt{-2\tilde{E}}-\frac{\tilde{F}}{4\tilde{E}}(3\lambda_\xi^2+\tau). \tag{3.6}$$

In order to solve the scaled differential equation for $\tilde{Y}_{MA}(\tilde{\eta})$, we define the regions $\mathcal{A}_1$ and $\mathcal{A}_2$ on the $\tilde{\eta}$ axis [see Fig. 2(a)], which contain the turning points $\tilde{\eta}_1$ and $\tilde{\eta}_2$, respectively. In that case the etalon equation method can be applied separately in the regions $\mathcal{A}_1$ and $\mathcal{A}_2$.

In the ''atomic'' region $\mathcal{A}_1$, we have

$$\tilde{Y}^{(1)}_{MA}(\tilde{\eta})=\frac{\tilde{A}}{\sqrt{u'}}M_{\lambda,m/2}(bu),\quad \tilde{\eta}\in\mathcal{A}_1, \tag{3.7}$$

where $\tilde{A}$ is a constant and $u'(\tilde{\eta})=du(\tilde{\eta})/d\tilde{\eta}$. The variable u is determined by

$$u(\tilde{\eta})=\int_0^{\tilde{\eta}}p\,d\tilde{\eta}+\frac{2\lambda}{b}\left[\int_0^{\tilde{\eta}}p\left(\int_0^{\tilde{\eta}}p\,d\tilde{\eta}\right)^{-1}d\tilde{\eta}-p(0)\int_0^{\tilde{\eta}}(p\tilde{\eta})^{-1}d\tilde{\eta}\right]+O\left(\frac{1}{b^2}\right), \tag{3.8}$$

whereas the spectral parameter $\tilde{\lambda}$, Eq. (3.2c), is given by

$$\tilde{\lambda}=\lambda p(0)+\frac{p'(0)}{bp(0)}(3\lambda^2+\tau)+O\left(\frac{1}{b^2}\right). \tag{3.9}$$

The results presented up to now enable us to determine the etalonic spectral parameter:

$$\lambda = p^{-1}(0)\lambda_M + O(1/b), \quad \lambda_M = \frac{Z}{\gamma} - \left(n_1 + \frac{m+1}{2}\right). \tag{3.10}$$

The solution $\tilde{Y}^{(2)}_{MA}(\tilde{\eta})$ in the region $\mathcal{A}_2$, encompassing the turning point $\tilde{\eta}_2$, is given by

$$\tilde{Y}^{(2)}_{MA}(\tilde{\eta}) = \frac{\tilde{C}}{\sqrt{\sigma'}}\,[\mathrm{Ai}(b^{2/3}\sigma) + C\ \mathrm{Bi}(b^{2/3}\sigma)], \quad \tilde{\eta} \in \mathcal{A}_2, \tag{3.11}$$

where $\tilde{C}$ and C are constants and $\sigma'(\tilde{\eta}) = d\sigma(\tilde{\eta})/d\tilde{\eta}$, whereas $\mathrm{Ai}(x)$ and $\mathrm{Bi}(x)$ denote the Airy functions. For the function $\sigma(\tilde{\eta})$ we get

$$\sigma(\tilde{\eta}) = \left(\frac{3}{4}\int_{\tilde{\eta}_2}^{\tilde{\eta}} p\ d\tilde{\eta}\right)^{2/3} - \frac{\lambda p(0)}{b}\left(\frac{3}{4}\int_{\tilde{\eta}_2}^{\tilde{\eta}} p\ d\tilde{\eta}\right)^{-3/4} \times \int_{\tilde{\eta}_2}^{\tilde{\eta}} (p\tilde{\eta})^{-1} d\tilde{\eta} + O\left(\frac{1}{b^2}\right). \tag{3.12}$$

The obtained solutions $\tilde{Y}^{(1)}_{MA}(\tilde{\eta})$ and $\tilde{Y}^{(2)}_{MA}(\tilde{\eta})$ have to match smoothly in the subbarrier region $\mathcal{A} = \mathcal{A}_1 \cap \mathcal{A}_2$ [see Fig. 2(a)]; in other words, we impose the following two matching conditions:

$$\tilde{Y}^{(1)\prime}_{MA}\tilde{Y}^{(2)}_{MA} = \tilde{Y}^{(1)}_{MA}\tilde{Y}^{(2)\prime}_{MA}, \quad \tilde{\eta} \in \mathcal{A}, \tag{3.13a}$$

$$\tilde{Y}^{(1)}_{MA} = \tilde{Y}^{(2)}_{MA}, \quad \tilde{\eta} \in \mathcal{A}. \tag{3.13b}$$

According to the standard procedure of the etalon equation method,[14] for the functions $\tilde{Y}^{(1)}_{MA}(\tilde{\eta})$ and $\tilde{Y}^{(2)}_{MA}(\tilde{\eta})$ in Eqs. (3.13a) and (3.13b) we can use their asymptotic forms.

From Eq. (3.7) we see that the asymptotic form of the function $\tilde{Y}^{(1)}_{MA}(\tilde{\eta})$ for $\tilde{\eta} \in \mathcal{A}$ is determined by the asymptotic expansion of the Whittaker function $M_{\lambda,m/2}(bu)$. We realized that with an appropriate choice of the asymptotic form of this function, the following fact appears: in the case of Rydberg-level population of multiply charged ions, not only the argument *bu* but also the first index λ can be considered as a large parameter. Indeed, for Rydberg states of multiply charged ions ($Z \gg 1$), the values of $\lambda \sim Z$, Eq. (3.10), will also be large (for the most relevant values $n_1 = 0$ and $m = 0$).

It is known[16] that asymptotic forms of the Whittaker function $M_{\lambda,m/2}(bu)$ depend on the relative order of the argument and the first index; more precisely, the character of the asymptotic expansions is determined by the ratio $u_s(\tilde{\eta}) = bu(\tilde{\eta})/4\lambda$. For $u_s(\tilde{\eta}) \geqslant 1$, we must explicitly use two-large-parameter asymptotics[16] of the Whittaker function. However, if $u_s(\tilde{\eta}) \gg 1$, the argument *bu* of $M_{\lambda,m/2}(bu)$ can be considered as a much larger quantity in comparison to the first index λ. In that sense, instead of two-large-parameter asymptotics, it is sufficient to use a one-large-parameter asymptotic expansion,[17] i.e., we can take that only the argument *bu* represents a large parameter.

The mentioned asymptotic forms can be related to the scaling parameter α. Namely, for $\tilde{\eta} \in \mathcal{A}$ we have $u_s(\tilde{\eta}) \approx \frac{1}{2}(1+\alpha)$. Therefore, in the close turning points configuration ($\alpha \approx \alpha_0 \approx 1$) we have $u_s(\tilde{\eta}) \approx 1$ and, consequently, for the asymptotic form of the function $\tilde{Y}^{(1)}_{MA}(\tilde{\eta})$ we must use the expression obtained by means of two-large-parameter asymptotics of the Whittaker function $M_{\lambda,m/2}(bu)$. Denoting the gamma function by $\Gamma(\cdots)$, we have

$$\tilde{Y}^{(1,I)}_{MA}(\tilde{\eta}) = \frac{\tilde{A}A}{\sqrt{u'}}\,[B_1(\lambda,u_s)e^{2f_1\lambda}f_2^{-2\lambda} + B_2(\lambda,u_s)e^{-2f_1\lambda}f_2^{2\lambda}], \tag{3.14a}$$

where $A(u_s) = \Gamma(m+1)(1-1/u_s)^{-1/4}$ and

$$B_1(\lambda,u_s) \approx \Gamma^{-1}\left(\frac{m+1}{2} - \lambda\right)\left(\frac{\lambda}{e}\right)^{-\lambda}, \tag{3.14b}$$

$$B_2(\lambda,u_s) \approx \Gamma^{-1}\left(\frac{m+1}{2} + \lambda\right)\left(\frac{\lambda}{e}\right)^{\lambda}\exp\left[\pm i\pi\left(\lambda - \frac{m+1}{2}\right)\right], \tag{3.14c}$$

whereas $f_1(u_s) = [u_s(u_s-1)]^{1/2}$ and $f_2(u_s) = u_s^{1/2} + (u_s - 1)^{1/2}$.

On the other hand, the distant turning points case ($\alpha \gg \alpha_0$) is associated with $u_s(\tilde{\eta}) \gg 1$, so that as a sufficiently good asymptotic form of $\tilde{Y}^{(1)}_{MA}(\tilde{\eta})$ we can use the expression obtained by one-parameter asymptotics:

$$\tilde{Y}^{(1,II)}_{MA}(\tilde{\eta}) = \frac{\tilde{A}}{\sqrt{u'}}\,\Gamma(m+1)\left[\Gamma^{-1}\left(\frac{m+1}{2} - \lambda\right) \times \left(\frac{\lambda}{e}\right)^{-\lambda} e^{2f_{10}\lambda} f_{20}^{-2\lambda} + \cdots\right], \tag{3.15}$$

where $f_{10}(u_s) = u_s - 1/2$ and $f_{20}(u_s) = 2u_s^{1/2}$.

The proposed asymptotic forms of the functions $Y^{(1,I)}_{MA}$ and $Y^{(1,II)}_{MA}$ will differ exclusively with the values of α which are very close to $\alpha_0 = \alpha_0(Z)$.

The asymptotic form of $\tilde{Y}^{(2)}_{MA}$ in the matching region $\mathcal{A}$ is determined by the asymptotic behavior of the Airy functions $\mathrm{Ai}(b^{2/3}\tilde{\eta})$ and $\mathrm{Bi}(b^{2/3}\tilde{\eta})$ for sufficiently large argument $b^{2/3}\tilde{\eta}$:

$$\tilde{Y}^{(2)}_{MA}(\tilde{\eta}) = \frac{\tilde{C}C}{\sqrt{\pi}}\,\frac{(b^{2/3}\sigma)^{1/4}}{\sqrt{\sigma'}}\left[\frac{(1-iC)}{2C}\,e^{-f_3} + e^{f_3}\right], \tag{3.16}$$

where $f_3 = \frac{2}{3}b\sigma^{2/3}$.

With the known asymptotic forms of $\tilde{Y}^{(1)}_{MA}(\tilde{\eta})$ and $\tilde{Y}^{(2)}_{MA}(\tilde{\eta})$ we can return to the first matching condition (3.13a), which will be transformed into an appropriate ''dispersion relation.'' Of course, since the function $\tilde{Y}^{(1)}_{MA}(\tilde{\eta})$ has two asymptotic forms corresponding to $\alpha \approx \alpha_0$ and $\alpha \gg \alpha_0$, we obtain two different expressions for the dispersion relation. In the first of the mentioned cases we have

$$\sin\left[\pi\left(\frac{m+1}{2} - \lambda\right)\right] = \frac{C}{1-iC}\exp\left[\pm i\pi\left(\frac{m+1}{2} - \lambda\right)\right]D(\lambda), \tag{3.17a}$$

where

$$D(\lambda) = e^{-4f_1\lambda}f_2^{4\lambda}e^{2f_3}. \tag{3.17b}$$

A similar dispersion relation follows from the condition (3.13a) for $\alpha \gg \alpha_0$; the only change consists in replacing the function $D(\lambda)$ of Eq. (3.17a) by the function $D_0(\lambda)$:

$$D_0(\lambda) = e^{-4f_{10}\lambda} f_{20}^{4\lambda} e^{2f_3}. \tag{3.17c}$$

The second matching condition, Eq. (3.13b), enables us to express the constant $\tilde{A}$ in terms of the constants C and $\tilde{C}$. For $\alpha \approx \alpha_0$, we have the following relation:

$$\tilde{A} = \tilde{C} C \left(\frac{2}{\pi}\right)^{1/2} b^{-1/6} \frac{\Gamma\left(\frac{m+1}{2} - \lambda\right)}{\Gamma(m+1)} \left(\frac{\lambda}{e}\right)^{\lambda} \left(1 - \frac{1}{u_s}\right)^{1/4} D^{1/2}(\lambda). \tag{3.18}$$

The expression (3.18) also holds for $\alpha \gg \alpha_0$, but instead of $(1-1/u_s)^{1/4} D^{1/2}(\lambda)$ we must take $D_0^{1/2}(\lambda)$.

C. Energy eigenfunctions $\Phi_{MA}^{(I)}$ and $\Phi_{MA}^{(II)}$

As a consequence of the applied matching procedure, two different classes of the eigenfunctions Φ_{MA} must be distinguished: in the case of close turning points configuration ($\alpha \approx \alpha_0$) we shall have the functions $\Phi_{MA}^{(I)}$, whereas for distant turning points configuration ($\alpha \gg \alpha_0$) the functions $\Phi_{MA}^{(II)}$ will be relevant.

Recalling Eqs. (2.2) and (3.5), we have

$$\Phi_{MA}^{(I)} = \frac{e^{\pm i m \varphi}}{\sqrt{\xi \eta}} M_{n_1 + (m+1)/2, m/2}(\gamma \xi) \tilde{Y}_{MA}^{(I)}(\tilde{\eta}), \tag{3.19}$$

where $\tilde{Y}_{MA}^{(I)}(\tilde{\eta})$ is expressed by $\tilde{Y}_{MA}^{(1)}(\tilde{\eta})$ for $\tilde{\eta} \in \mathcal{A}_1$ and by $\tilde{Y}_{MA}^{(2)}(\tilde{\eta})$ for $\tilde{\eta} \in \mathcal{A}_2$, Eqs. (3.7) and (3.11), respectively. We determined the constant $\tilde{C}$ by a normalization procedure, based on the eigendifferential technique:[18]

$$|\tilde{C}| = \left[\frac{(m+n_1)!}{n_1! m!^2}\right]^{1/2} \frac{b^{1/6}}{[2\pi f(\lambda)]^{1/2}} \frac{1}{|C|}, \tag{3.20a}$$

where

$$f(\lambda) = 2 + \frac{D^2(\lambda)}{4 \sin^2\left[\pi\left(\lambda - \frac{m+1}{2}\right)\right]}, \tag{3.20b}$$

whereas C is determined by the dispersion relation (3.17a). With the constant $\tilde{C}$ known, we completed the eigenfunction $\Phi_{MA}^{(I)}$ on the entire $\tilde{\eta}$ axis.

In our subsequent discussions, however, we need the function $\Phi_{MA}^{(I)}$ exclusively on the Firsov plane S_F. As we can see in the context of quantum dynamics (Sec. IV), the moving S_F plane is positioned in the $\mathcal{A}_1$ region [see Fig. 2(a)]. Therefore, an expression for $\Phi_{MA}^{(I)}$ on the S_F plane can be obtained from Eq. (3.19) by setting $\tilde{Y}_{MA}^{(I)}(\tilde{\eta}) = \tilde{Y}_{MA}^{(1)}(\tilde{\eta})$. However, such a formula for $\Phi_{MA}^{(I)}$ would be expressed in terms of the Whittaker function $M_{\lambda, m/2}(bu)$, so that our further analysis would be possible on a numerical level exclusively. This numerical approach is not suitable for our quantum dynamic considerations, where we need a sufficiently simple and plausible analytic expression for $\Phi_{MA}^{(I)}$ on the S_F plane which will be correct for all parameters of the system (γ, n, l, R, Z).

An appropriate asymptotic expression for the function $\Phi_{MA}^{(I)}$ on the S_F plane can be obtained through a procedure of analytic continuation of the already known asymptotic form of that function in the matching region $\mathcal{A}$. As a result we have the following form of the function $\Phi_{MA}^{(I)}$ on the S_F plane and for $\alpha \approx \alpha_0$:

$$\Phi_{MA}^{(I)} = N_\gamma R^{\alpha_{1R}} a^{\alpha_a} e^{-\tilde{\gamma} z}, \tag{3.21}$$

where

$$\tilde{\gamma} = \frac{\gamma}{\sqrt{C_0}} \left(1 + \frac{3}{4\alpha}\right), \quad C_0 = 1 + \frac{3}{2\alpha}, \tag{3.22a}$$

and

$$\alpha_{1R} = \frac{1}{\sqrt{C_0}} \left[\lambda_M + \frac{1}{4\gamma C_0}\left(1 + \frac{9}{4\alpha}\right)\right], \tag{3.22b}$$

$$\alpha_a = \frac{1}{\sqrt{C_0}} \left(-\lambda_M - \frac{\sqrt{C_0}}{2}\right). \tag{3.22c}$$

The quantity N_γ is given by

$$N_\gamma = \frac{1}{\pi\sqrt{2f}} C_0^{-1/4} \gamma^{1/2 + 2N_1} e^{N_2} 2^{N_1 - Z/(\gamma\sqrt{C_0})} (2\sqrt{C_0})^{2N_1}, \tag{3.23}$$

where

$$N_1 = \frac{1}{4\gamma C_0 \sqrt{C_0}} \left(1 + \frac{9}{4\alpha}\right) \tag{3.24a}$$

and

$$N_2 = \frac{1}{4\gamma C_0 \sqrt{C_0}} \left(1 + \frac{3}{4\alpha}\right). \tag{3.24b}$$

The expression for N_γ can be simplified if we take into account that $D(\lambda) \ll 1$. In that case, from Eq. (3.20b) we get $f(\lambda) \approx 2$, for all values of $\lambda \neq \lambda_A$, where $\sin\{\pi[\lambda_A - (m+1)/2]\} = 0$. Let us note that $\Phi_{MA}^{(I)}$ is proportional to $(a/R)^{m/(2\sqrt{C_0})}$, where $a/R \approx 1/2$. Accordingly, with the leading term in the transition probability T_{nl}, we have $m = 0$.

What remains is to find an appropriate expression for the energy eigenfunction $\Phi_{MA}^{(II)}$ on the S_F plane, responsible for the case of distant turning points configuration ($\alpha \gg \alpha_0$). For that purpose we note that the above-described procedure can be repeated step by step, keeping in mind that instead of the asymptotic expression given by (3.14a) we must use the asymptotics described by Eq. (3.15). In this way, we obtain

$$\Phi_{MA}^{(II)} = N_{\gamma 0} R^{\lambda_M + 1/(4\gamma)} a^{-\lambda_M - 1/2} e^{-\gamma z}, \tag{3.25a}$$

where

$$N_{\gamma 0} = \frac{1}{2\pi} \gamma^{1/2 + 1/(2\gamma)} (2e)^{1/(4\gamma)} 2^{-Z/\gamma + 1/(2\gamma)}. \tag{3.25b}$$

Expression (3.25) coincides with the asymptotic form (large R) of the Φ_{MA} function obtained previously[9] within the framework of JWKB method.

D. Energy eigenfunctions $\Phi_{AM}^{(I)}$, $\Phi_{AM}^{(II)}$, and $\Phi_{AM}^{(III)}$

We shall first discuss the parabolic eigenfunctions $\Phi_{AM}(\xi,\eta,\varphi)$. Using the same scaling procedure in Eq. (2.1b) as in the case of Eq. (2.1a), all considerations of Sec. III B can be repeated step by step.

As an output of these calculations, we obtain a dispersion relation in which the outgoing behavior of the considered function is taken into account. The explicit expression for that dispersion relation has a form given by Eq. (3.17a), but we must take $C=i$ instead of the constant C. Also, an atomic spectral parameter, denoted by λ_A, must be used instead of λ. The values of the functions $D(\lambda_A)$ and $D_0(\lambda_A)$ for both close and distant turning points configuration cases, Eqs. (3.17b) and (3.17c), represent exponentially small quantities again. Accordingly, a new dispersion relation is satisfied exclusively for a set of discrete values of the parameter $\lambda_A = n_{2A}+(m_A+1)/2$, where $n_{2A}=0,1,2,\ldots$ represents the second parabolic quantum number. The obtained values of etalonic spectral parameter λ_A enable us to reproduce the well-known asymptotic expression for the atomic energy levels $E_A=-\gamma_{A0}^2/2+\Delta E$, where $\gamma_{A0}=Z/n$. In that sense, the ion-surface distance R_F is given by $R_F=(Z-1/2)/(\gamma_{A0}^2-2\phi)$.

As in the case of the Φ_{MA} function, the explicit expressions for the functions $\Phi_{AM}(\xi,\eta,\varphi)$ depend on the turning points configuration, described by the scaling parameter $\alpha_A = -2E_AR/(Z-1/4)$. In the cases of close and distant turning points, we have the parabolic functions $\Phi_{AM}^{(I)}$ and $\Phi_{AM}^{(II)}$, respectively. These eigenfunctions are determined by Eq. (3.19), but instead of m, n_1, and γ we must take m_A, n_{1A}, and γ_A, where $n_{1A}+n_{2A}+m_A+1=n$.

The time-decay process of the parabolic eigenstates $\Phi_{AM}^{(I,II)}$ for $R<R_F$ is described by the ionization rates $\Gamma_\mu^{\rm ion}(R)$, Eq. (2.4). In order to obtain the quantity $\Gamma_\mu^{\rm ion}(R)$ for the function $\Phi_{AM}^{(I)}$, we start from the dispersion relation for the etalonic spectral parameter λ_A. Recalling that this relation has the same form as Eq. (3.17a), except in $C=i$, we consider the etalonic spectral parameter λ_A as a complex quantity, i.e., we take $\lambda_A\rightarrow\check{\lambda}_A=\lambda_A-i\delta$. Supposing that $\delta=-{\rm Im}(\check{\lambda}_A)\ll 1$, we get

$$\Gamma_\mu^{\rm ion}(R)\approx\frac{Z^2}{\pi n^3}D(\lambda_A), \tag{3.26}$$

where $D(\lambda_A)$ is determined by Eq. (3.17b). The expression (3.26) holds also for the function $\Phi_{AM}^{(II)}$, but instead of $D(\lambda_A)$ we have to take $D_0(\lambda_A)$; see Eq. (3.17c). By means of the obtained ionization rates $\Gamma_\mu^{\rm ion}(R)$ we can verify that the fast ionization condition, Eq. (2.9), is satisfied for all experimentally tested ions. For example, by testing the Cl VII case with $v=2.50$, $n=11$, and $l=1$ we found $\mathcal{E}\approx 0.3$, for $t\rightarrow\infty$, so that we can take $\mathcal{E}\ll 1$.

The spherical solutions $\Phi_{AM}(r,\theta,\varphi)=\Phi_{AM}^{(III)}$ of the eigenproblem (2.1b) are already known [Eq. (3.17a) of Ref. 9]. On the Firsov plane we have

$$\Phi_{AM}^{(III)}=N_{A0}a^{Z/\gamma_{A0}-1}e^{-\gamma_{A0}r_A}. \tag{3.27a}$$

For convenience we express the constant N_{A0} in the form

$$N_{A0}=\tilde{N}_{A0}S_{nl}(2\gamma_{A0}\sqrt{R^2+\rho^2}), \tag{3.27b}$$

where ρ represents the radial coordinate on the S_F plane. In expression (3.27) we restricted ourselves to the states with $m_A=0$. Namely, due to the orthogonality of the states Φ_{MA} and Φ_{AM} with respect to the ϕ variable, only the states $m_A=m$ could be populated. On the other hand, the solid valence-band states with $m=0$ are dominant in the electron-capture process we are considering [see the comment concerning the expression (3.21)].

IV. CALCULATION OF THE POPULATION PROBABILITY P_{nl}

The results obtained up to now enable us to explicate our final dynamic picture of the Rydberg-state population process, as well as to calculate the experimentally verifiable population probability $P_{nl}(v,Z)$. In Secs. IV A and IV B we shall perform the calculations considering the electron-capture dynamics without ionization. The consequences of the ionization activity are discussed in Secs. IV C and IV D.

A. Classification of the electron transitions and the mixed flux $I(t)$

The electron-capture flux $I(t)=I_{nl}^{\gamma}(t)$ is adopted for a description of the nonresonant electron-capture processes into the ionic Rydberg states (n,l). For that reason, at intermediate stages of the ion-surface interaction we can speak only about a kind of electron ''transition'' from the state $\Psi_M^{\gamma}(t)$ to the state $\Psi_A^{nl}(t)$, which are not the states of well-defined energies. Only the molecularlike eigenstates Φ_{MA} and Φ_{AM} are the components of the mixed flux with definite, but generally different, energies.

An additional fact characterizing the nonadiabatic approach based on the mixed flux $I_{nl}^{\gamma}(t)$ is that this quantity represents a very complicated function of time t and energy parameter γ. According to the values of the scaling parameter α, Eq. (3.2a), associated to each point of the γt plane, we can distinguish between two regions, satisfying either the condition $\alpha<\alpha_0$ or $\alpha>\alpha_0$. In the first case the turning points $\tilde{\eta}_1$ and $\tilde{\eta}_2$ will be complex, and the second region is characterized by the real values of the turning points. We adopted the following terminology: we define the overbarrier electron transitions by the requirement $\alpha<\alpha_0$, whereas the condition $\alpha>\alpha_0$ will be associated with the underbarrier transitions.

We realized that all points of the γt plane will not contribute to the electron-capture process in the same degree and that a self-consistent procedure can indicate those regions where the process is dominant. Namely, around the critical ion-surface distances $R_c=vt_c$, the main contribution to the transition probability $T_{nl}^{\gamma}(t)$, Eq. (2.6), can be expected from those solid valence-band states positioned around $\gamma\approx\gamma_{\max}$, where $\gamma_{\max}$ denotes the maximum of the function $T_{nl}^{\gamma}(t)$ on the γ scale. In other words, a dominant contribution comes from the vicinity of the point $(\gamma_{\max},t_c)$, so that a classification of the relevant expressions for the mixed flux I_{nl}^{γ} can be

performed according to the values $\alpha_c=\alpha(\gamma_{\max},t_c)$ of the scaling parameter α. The position of the point $(\gamma_{\max},t_c)$ as well as the value of α_c at that point depend on the ionic parameters n, l, Z, and v. For the experimentally tested parameters only the cases $\alpha_c\approx\alpha_0$ and $\alpha_c\gg\alpha_0$ appear, which can be interpreted (in the sense mentioned above) as an electron ''tunneling'' in the vicinity of the potential barrier top and a deep underbarrier ''tunneling,'' respectively.

In the case $\alpha\approx\alpha_0$, the mixed flux formula can be obtained by using the parabolic energy eigenstate $\Phi_{MA}^{(I)}$ and the spherical eigenstate $\Phi_{AM}^{(III)}$ in order to obtain the functions $\Psi_M^{\gamma}(t)$ and $\Psi_A^{nl}(t)$. The choice of the $\Phi_{AM}^{(III)}$ function for the molecularlike atomic state Φ_{AM} is motivated by the fact that we neglect the activity of the ionization mechanism in the pure electron-capture dynamics, i.e., if the ionization were absent, the detectors of the optical spectroscopy would observe the spherical states (n,l). Thus,

$$I(t)=\frac{i}{2}\,e^{iwt}\left[\tilde{\gamma}+\gamma_{A0}+iv\left(1-2\frac{da}{dR}\right)\right]\times\int_0^{2\pi}\int_0^{\infty}\Phi_{AM}^{(III)*}\Phi_{MA}^{(I)}e^{f_A^*+f_M}\rho\;d\rho\;d\psi, \quad (4.1a)$$

where

$$w=\tfrac{1}{2}(\tilde{\gamma}^2-\gamma_{A0})^2-\tfrac{1}{2}v^2\left(1-2\frac{a}{R}\right). \quad (4.1b)$$

The space-time correction factors f_A and f_M are calculated beforehand within the asymptotic method of solving the Schrödinger equation.[9]

Using the mean value theorem around the point $\rho_0=n^2/[Z(l+1)]$, we get

$$I(t)=\frac{i\pi e^{iwt}}{\gamma_{A0}^2}\,N(R)\left[\tilde{\gamma}+\gamma_{A0}+iv\left(1-2\frac{da}{dR}\right)\right]\times(1+\gamma_{A0}a)e^{(\tilde{\gamma}-\gamma_{A0})a}e^{-\tilde{\gamma}R}, \quad (4.2)$$

where

$$N(R)=\tilde{N}_0R^{\alpha_R}S_{nl}(2\gamma_{A0}\sqrt{R^2+\rho_0^2}) \quad (4.3a)$$

and

$$\tilde{N}_0=\tilde{N}_{A0}^*N_{\gamma}\left(\frac{a}{R}\right)^{Z/\gamma_{A0}-3/2-\lambda_M/\sqrt{C_0}}\exp(f_A^*+f_M). \quad (4.3b)$$

The exponent α_R appearing in Eq. (4.3a) is determined by

$$\alpha_R=\frac{Z}{\gamma_{A0}}-\frac{3}{2}+\frac{1}{4\gamma C_0^{3/2}}\left(1+\frac{9}{4\alpha}\right). \quad (4.3c)$$

The calculated mixed electron flux $I(t)$, Eq. (4.2), represents a functional of the Firsov plane position $\alpha=gR$, where g has the same form as in Ref. 9, but with $\tilde{\gamma}$ instead of γ.

In the case $\alpha\gg\alpha_0$, the relevant formula for the mixed flux is constructed by means of the energy eigenfunctions $\Phi_{MA}^{(II)}$ and $\Phi_{AM}^{(III)}$. Its explicit form is described by the expression (4.2), but with C_0, α_R, N_{γ}, and $\tilde{\gamma}$ transformed as follows:

$$C_0\to 1,\quad \alpha_R\to\frac{Z}{\gamma_{A0}}-\frac{3}{2}+\frac{1}{4\gamma},\quad N_{\gamma}\to N_{\gamma 0},\quad \tilde{\gamma}\to\gamma. \quad (4.4)$$

It is worth noting that such an expression for $I(t)$ has the same form as in our previous paper based on the JWKB approximation.[9]

B. Transition rate $\tilde{\Gamma}_{nl}^{\gamma}(R)$ and resonant quantum numbers $n_{\rm res}$

In order to concretize the type of electron transitions and to define the resonant quantum number $n_{\rm res}$, we need to estimate first the critical ion-surface distances R_c by evaluating the transition rate $\tilde{\Gamma}_{nl}^{\gamma}(R)$, Eq. (2.7).

For $\alpha\approx\alpha_0$ the transition rate $\tilde{\Gamma}_{nl}^{\gamma}$ as a function of R is characterized by the bell-shaped maxima, placed at the ion-surface distances R_c with characteristic half-widths ΔR. We found that a sufficiently good estimation can be given by

$$R_c\approx 2\kappa(n,l,v)R_m,\quad R_m=\frac{\alpha_R}{\gamma_{A0}g+\tilde{\gamma}(1-g)}, \quad (4.5)$$

where $\kappa(n,l,v)$ represents a modulating function, weakly dependent on the principal quantum number n. In the case of the low angular momentum Rydberg states ($l=0$, 1, and 2), we found as the best fit

$$\kappa(n,l,v)=0.744\left(1+0.298\frac{\kappa_l}{v}\right)\left(1+\frac{1}{4n}\right), \quad (4.6)$$

where the parameter κ_l is determined by $\kappa_0=1$ and $\kappa_1=\kappa_2=2$. Our explicit numerical calculations showed that $\Delta R\approx 7$ a.u., for all experimentally relevant values of the parameters.

The ''critical'' values $\alpha_c=\alpha(R_c)$ of the scaling parameter α are very sensitive to the change of principal quantum number n. For the Rydberg states (n,l) populating in the close turning points configuration, the values of the scaling parameter α_c satisfy the condition

$$\alpha_c=\frac{\gamma^2R_c(\alpha_c)}{Z-\frac{1}{4}}=\alpha_0. \quad (4.7)$$

We define the resonant quantum number $n_{\rm res}$ as an integer solution of Eq. (4.7). To obtain the quantity $n_{\rm res}$ it is not necessary to include all possible values of the parameter γ. Namely, in the case of a ''tunneling'' near the top of the potential barrier at $R=R_c$, we can take $\gamma\approx\gamma_F$, i.e., the main contribution arises from valence-band levels placed right below the E_F level.

The results of our numerical treatment of Eq. (4.7) are presented in Table I, where the relevant ionic velocities are taken from available experiments.[2–4] We used the value $\gamma_F=0.47$ a.u. as the energy parameter γ_F of the Fermi level E_F, corresponding to the work function $\phi=3$ eV. In Table I we see that the Rydberg resonances of Ar VIII with $l=1$ and 2 have $n=n_{\rm res}=11$ (which is in full agreement with the experimentally observed data[2]). On the other hand, the resonance of Ar VIII, with $l=0$ and $n=n_{\rm res}=12$ theoretically obtained on the basis of pure electron-capture calculations by means of mixed flux $I(t)$, has not been detected in experi-

TABLE I. Low angular momentum values of the resonant quantum number $n_{\rm res}$ for the ions of chlorine, sulfur, and argon (at experimentally tested velocities, v).

$n_{\rm res}$	S VI ($v=1.94$)	Cll VII ($v=2.50$)	Ar VIII ($v=1.42$)
$l=0$	11	12	12
$l=1$	10	11	11
$l=2$	10	11	11

ments. The theoretically obtained resonances are also absent in the case of S VI and Cl VII for all low values of l.

In order to develop our electron-capture dynamics without ionization for the case $\alpha \gg \alpha_0$, we calculated the transition rate $\tilde{\Gamma}^{\gamma}_{nl}(R)$, using the second expression for the mixed flux, mentioned in Sec. IV A. This procedure results again in the bell-shaped maxima of the quantity $\tilde{\Gamma}^{\gamma}_{nl}(R)$ as a function of R: the maxima positions at $R=R_c$ are given by Eq. (4.5), but with the transformation (4.4) applied.

C. Transition probability T^{γ}_{nl} and threshold quantum numbers $n_{\rm thr}$

From the standpoint of detection by the methods of optical spectroscopy, only those Rydberg states (including resonances) whose formations take place dominantly at $R_c > R_F$ (i.e., when E_A is below the Fermi level E_F) will survive and be experimentally registered. In Fig. 3(a) we presented this process schematically. On the other hand, all Rydberg states dominantly formed above E_F, i.e., under the condition $R_c < R_F$, will be destroyed fast by ionization and will not be observed in the beam-foil experiments, Fig. 3(b).

The presented structure of the processes follows from an analysis of the transition probability T^{γ}_{nl}, Eq. (2.10). Let us consider, first, the case leading to an observable Rydberg state (n,l) populated dominantly below the Fermi level E_F so that the influence of the ionization effect can be neglected. Since in this case we have $R_c > R_F$, our calculation of the transition probability T^{γ}_{nl} will be performed by means of Eq. (2.10a).

In the configuration of close turning points ($n \approx n_{\rm res}$), i.e., for $n \in \mathcal{N}_r$, a relevant formula for the population probability T^{γ}_{nl} can be obtained by inserting Eq. (4.2) into Eq. (2.10a). We get

$$T^{\gamma}_{nl} = T|\tau^{\gamma}_{nl}|^2, \quad R_c > R_F, \quad n \in \mathcal{N}_r, \tag{4.8}$$

where

$$T = \frac{\pi^2}{\gamma_{A0}^4}\, g^{2n_1/\sqrt{C_0}} |\tilde{N}_{A0}|^2 |N_{\gamma}|^2 \mathcal{T}^2(g)[(\tilde{\gamma}+\gamma_{A0})^2 + v^2(1-2g)^2] S^2_{nl}(4n) \tag{4.9a}$$

and

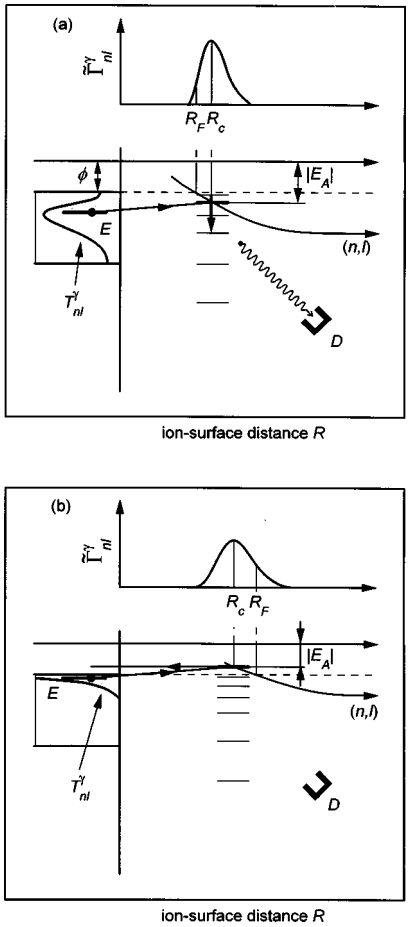

FIG. 3. The population process of Rydberg states (n,l) for $R_c > R_F$ ($|E_A| > \phi$) and $R_c < R_F$ ($|E_A| < \phi$). (a) Electron-capture process followed by photon deexcitation. (b) Electron-capture process followed by ionization decay of a ionic Rydberg state.

$$\mathcal{T} = g^{Z/\gamma_{A0} - (Z/\gamma - 1/2)/\sqrt{C_0} - 3/2} (1-g)^{v^2/[4\gamma_{A0}(\gamma_{A0}^2+v^2)]} \times \left(1-\frac{g}{2}\right)^{-4Zv^2/[\gamma_{A0}(\gamma_{A0}^2+4v^2)]} \times [g(2-g)]^{Zv^2/[\tilde{\gamma}(\tilde{\gamma}^2+v^2)]} e^{-(2Z-1)g/(4\gamma_{A0})}. \tag{4.9b}$$

The quantity $|\tau^{\gamma}_{nl}|^2$ is defined by

$$|\tau^{\gamma}_{nl}|^2 = v^{2\alpha_R}\Gamma^2(\alpha_R+1)\, \frac{[\gamma_{A0} g(\alpha_R+1)v + \Omega]^2 + w^2}{(\Omega^2+w^2)^{\alpha_R+2}}, \tag{4.10a}$$

where

$$\Omega = [\tilde{\gamma}(1-g) + \gamma_{A0} g]v. \tag{4.10b}$$

Taking into account that the quantity T^{γ}_{nl} as a function of n decreases rapidly in the region $n > n_{\rm res}$, the obtained expression can be used in the calculation of the transition probabilities for $n \gtrsim n_{\rm res}$.

In the configuration of distant turning points ($n \in \mathcal{N}$), the relevant expression for T^{γ}_{nl} has the same form as given by Eqs. (4.8), (4.9), and (4.10), but with the parameters C_0, c,

TABLE II. Low angular momentum values of the threshold quantum number $n_{\rm thr}$ for the ions of chlorine, sulfur, and argon (at experimentally tested velocities, v).

$n_{\rm thr}$	S VI ($v=1.94$)	Cl VII ($v=2.50$)	Ar VIII ($v=1.42$)
$l=0$	8	9	11
$l=1$	8	9	12
$l=2$	8	9	12

N_γ, and $\tilde{\gamma}$ transformed in accordance with Eq. (4.4). In this way, we arrive at an expression for T_{nl}^{γ} which is applicable for $n<n_{\rm res}$.

What remains is to consider the population probability T_{nl}^{γ} of the Rydberg levels dominantly formed and destroyed above the Fermi level E_F. In this case the calculation of T_{nl}^{γ} must be performed by means of Eq. (2.10b). We obtain

$$T_{nl}^{\gamma}=T|J_{nl}^{\gamma}|^2;\ \ R_c<R_F,\quad n\in\mathcal{N}_r, \tag{4.11a}$$

where T is given by Eq. (4.9a) with $S_{nl}(2R_F)$ instead of $S_{nl}(4n)$ and

$$|J_{nl}^{\gamma}|^2=\frac{R_F^{2\alpha_R}\exp\left(-\frac{2\Omega}{v}R_F\right)}{(\Omega^2+w^2)^2}\{[1+\gamma_{A0}gR_F+\gamma_{A0}g(\alpha_R+1)v]^2+w^2(1+\gamma_{A0}gR_F)^2\}. \tag{4.11b}$$

The corresponding expression for T_{nl}^{γ} in the case $n\in\mathcal{N}$ is obtained after the transformation explicated by Eq. (4.4) has been done.

The activity of the threshold mechanism becomes evident by means of a numerical test of the expression (4.11a) for T_{nl}^{γ}. Namely, it turns out that the calculated values of T_{nl}^{γ} become negligible for all experimentally tested ions ($Z=6$, 7, and 8) with relevant velocities v and for all low-angular momentum cases ($l=0$, 1, and 2). In other words, we have $T_{nl}^{\gamma}\approx 0$ for $n>n_{\rm thr}$, where $n_{\rm thr}$ is the threshold quantum number. The quantity $n_{\rm thr}+1$ represents a minimal integer satisfying the condition $R_c\leqslant R_F$. The numerically obtained values of $n_{\rm thr}$ are presented in Table II.

An interplay of resonance and threshold phenomena can be seen if the results presented in Tables I and II are compared. It is clear that only the Ar VIII resonance levels $n=11$ for $l=1$ or 2 are observable. The other resonances obtained theoretically inside the electron-capture model exclusively (i.e., without taking their ionization into account) represent a set of short-lived Rydberg states, hidden for the optical spectroscopy measurements.

The formulas for the transition probability T_{nl}^{γ} enable us to elucidate the nonresonant character of the electron-capture process. Namely, the contributions of solid valence-band electrons in the process are different for different values of n, l, Z, and v. The γ dependence of T_{nl}^{γ} for Ar VIII with $l=1$ at an experimentally tested velocity ($v=1.42$) is presented in Figs. 4(a) and 4(b). Note the different T_{nl}^{γ} scales in Figs. 4(a) and 4(b). The T_{nl}^{γ} curves for $l=0$ of Ar VIII, as well as for

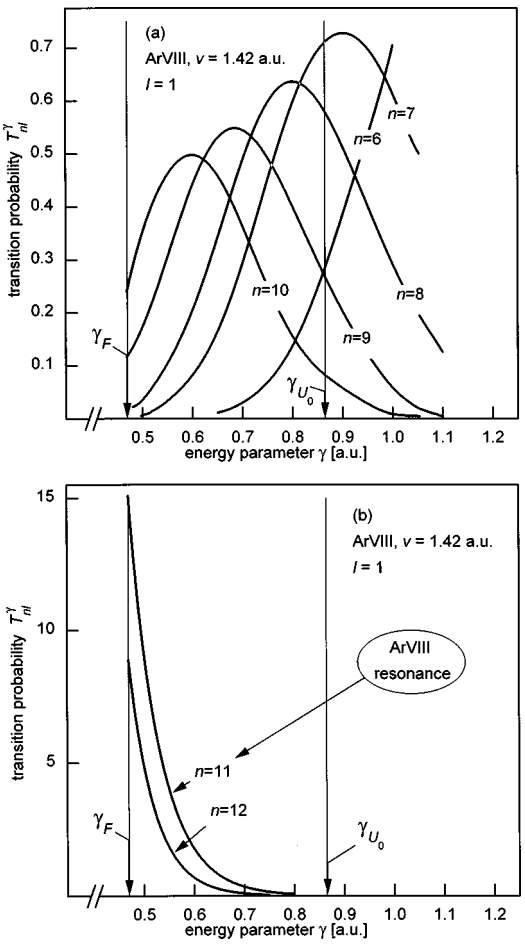

FIG. 4. Transition probabilities T_{nl}^{γ} (per unit γ) as a function of the energy parameter γ for Ar VIII ($v=1.42$ a.u.) ion, for $n\in\mathcal{N}, l=1$ and $n\in\mathcal{N}_r, l=1$, respectively.

the experimentally tested ions S VI and Cl VII with $l=0$, 1, and 2, are similar to those presented in Fig. 4(a).

It can be verified by direct numerical calculations that the positions of all maxima of the T_{nl}^{γ} curves are placed at the values $\gamma=\gamma_{\max}\approx\gamma_A(R_c)$. In other words, a quasiresonant ''kernel'' $\gamma_{\max}\rightarrow\gamma_A(R_c)$ can be recognized for all relevant values of the parameters n, l, Z, and v. This fact represents the main reason which motivated us to express the results of the quantum dynamics based on the mixed flux I_{nl}^{γ} in terms of the most frequently used concepts of the adiabatic and resonant theories (see Sec. IV A). The calculation of the α_c values shows that $\alpha_c>\alpha_0$, so that only the underbarrier kernels appear for the experimentally investigated ionic states.

D. Population probability P_{nl}

We finalize our study of Rydberg-state formation by an explicit calculation of the experimentally verifiable population probability $P_{nl}=P_{nl}(v,Z)$, determined by Eq. (2.11).

To do this, we need first to calculate the transition probability T_{nl} from all states of the foil conduction band to a Rydberg state (n,l). The summation over discrete quantum numbers is reduced to a summation over the parabolic quantum number n_1 and $m=m_A=0$ of the valence-band states, whereas the integration over energy parameter γ must be

taken from $\gamma=\sqrt{2\phi}$ to $\gamma_{U_0}=\sqrt{2U_0}$. As in our previous paper,[9] we take $U_0=10$ eV as the relevant value in the case of graphite foils.

In order to proceed from the probability T_{nl} to the experimentally verifiable multichannel population probability P_{nl}, Eq. (2.11), it is necessary to define a set of the background states (n',l') that ''interfere'' in the population process of the state (n,l). A suitable interference scheme follows from the analysis of the interference factors $p^{\gamma nl}_{n'l'}(t)$ appearing in our ϱ-matrix formalism.[9] We define the background states (n',l') of the state (n,l) as the states satisfying the condition $p^{nl}_{n'l'}(t)\neq 0$, where $p^{nl}_{n'l'}(t)$ stands for the value of the factor $p^{\gamma nl}_{n'l'}(t)$ averaged over the relevant values of the γ parameter.

The key points in an estimation of the $p^{nl}_{n'l'}(t)$ factors are the following facts. First, the population process of a given Rydberg state (n,l) is mainly finished at the time $\tau=t_c+\Delta R/v$; accordingly, the transition probability $T_{nl}(t)$ can be estimated by $T_{nl}(t)\approx T_{nl}\Theta(t-\tau)$, where $\Theta(t-\tau)$ denotes the Heaviside step function. Second, during the population process of the state (n,l), all electron-capture channels leading to the states (n',l') are open simultaneously; for the transition probability $T_{n'l'}(t)$ we can use the analogous steplike expression. Third, the mean values $p^{nl}_{n'l'}(t)$ can be expressed in terms of $T_{nl}(t)$ and $T_{n'l'}(t)$ exclusively. As a consequence of these facts, it turns out that the nonvanishing $p^{nl}_{n'l'}(t)$ values have those channels leading to the states (n',l'), populated around the critical ion-surface distances $R_c(n',l')$ smaller than $R_c(n,l)+\Delta R(n,l)$. Therefore, the values of the quantum numbers n' and l' of the relevant ''background'' states can be found by solving the inequality

$$R_c(n',l')\leqslant R_c(n,l)+\Delta R(n,l) \tag{4.12}$$

for any given set of the parameters n, l, Z, and v.

Having the set of relevant background states, we estimated the mean value $\langle T_{n'l'}\rangle_{l'}$, of the transition probability $T_{n'l'}$ over the angular momentum quantum numbers l' of the background states. Finally, for $l=0$ we obtain

$$P_{n0}=\tilde{P}_{n0}\exp\left(-\sum_{n'\neq n}^{n_{\rm res}(1)-1}T_{n'1}-\sum_{n'\geqslant n_{\rm res}(1),n'\neq n}T_{n'0}\right) \tag{4.13}$$

and, for $l=1$ and 2, we get

$$P_{nl}=\tilde{P}_{nl}\exp\left(-\sum_{n'\neq n}^{n_{\rm res}(1)-1}T_{n'1}\right);\quad n<n_{\rm res}(1), \tag{4.14a}$$

$$P_{nl}=\tilde{P}_{nl}\exp\left(-\sum_{n'\neq n}T_{n'1}\right);\quad n\geqslant n_{\rm res}(1), \tag{4.14b}$$

where $\tilde{P}_{nl}=1-\exp(-T_{nl})$. Relations (4.13) and (4.14) represent our final expressions for the population probability P_{nl}, which will be compared with available experimental data.[2–4] We normalize the experimental findings to the theoretical ones at the central population maxima $n=n_0\approx Z$, calculated in our previous paper.[9] The estimated overall uncertainty in the measured relative population probabilities is around 20% (see, e.g., Ref. 4).

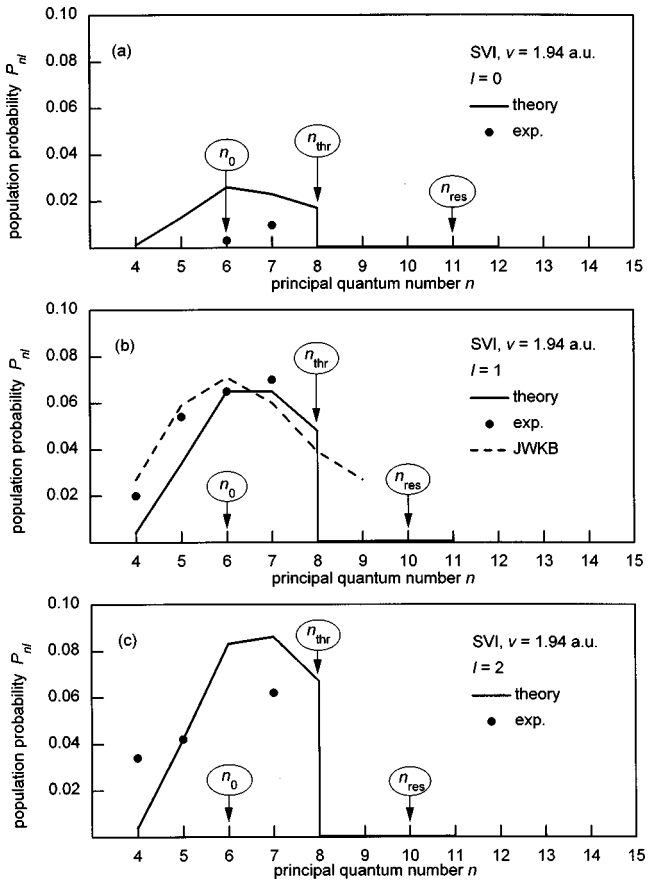

FIG. 5. Population probabilities P_{nl} of the Rydberg states (n,l) for S VI ion ($v=1.94$ a.u.) with $l=0$, 1, and 2, respectively. Dots are experimental data (Refs. 3 and 4).

In Fig. 5 we compared our theoretical predictions (full lines) for sulfur ions S VI with experimental findings[3,4] (dots), restricting ourselves to the low angular momentum cases ($l=0$, 1, and 2). The ionic energy used in the cited experiments is $E=3$ MeV, which corresponds to the velocity $v=1.94$ a.u. of the S VI ions. As we can see, the presented P_{nl} curves have ''ordinary'' shapes with maxima located at $n=n_0\approx Z$, but with thresholds at $n_{\rm thr}=8$. In the considered S VI case, the resonant quantum numbers are indicated by arrows positioned to the right from $n_{\rm thr}$, which explains the absence of observable resonances in the population curves. The dashed line indicated in Fig. 5(b) is taken from our previous paper:[9] obviously, for $n<n_{\rm thr}$ and $l=1$ the JWKB prediction correlates to the full P_{nl} curve of the present paper. The same correlation exists for $l=0$ and 2 of the S VI ions.

In Fig. 6 we presented our results for low l cases of Cl VII with experimentally[3,4] tested energy $E=5.5$ MeV ($v=2.50$ a.u.). The obtained P_{nl} curves (full lines) of the Cl VII ions are similar to those exposed in Fig. 5, but with thresholds at $n_{\rm thr}=9$ and resonant quantum numbers $n_{\rm res}=12$ and 11. Nevertheless, the inequality $n_{\rm res}>n_{\rm thr}$ holds, so that the Cl VII resonances are also hidden for the optical spectroscopy. The dashed JWKB curve for $l=1$ marked in

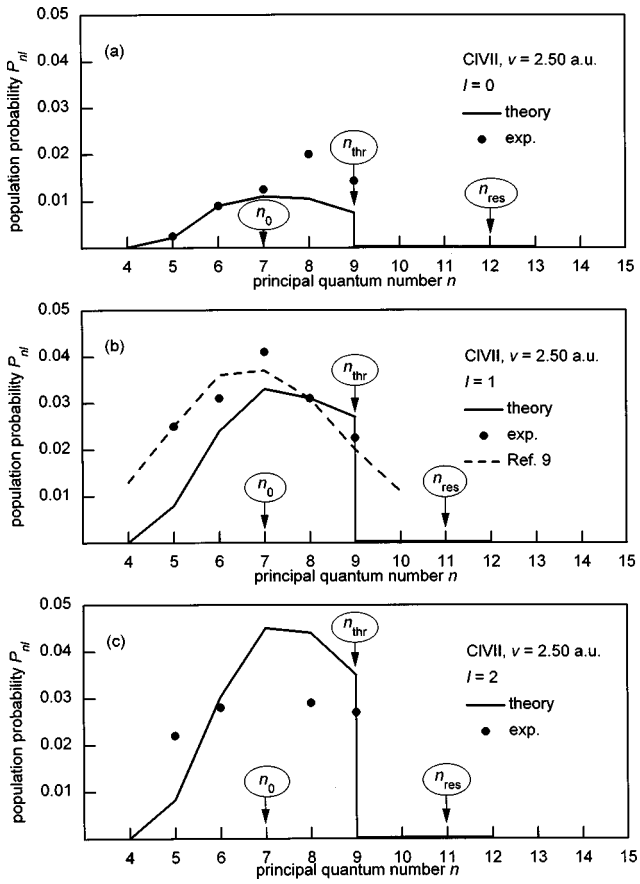

FIG. 6. Population probabilities P_{nl} of the Rydberg states (n,l) for Cl VII ion ($v=2.50$ a.u.) with $l=0$, 1, and 2, respectively. Dots are experimental data (Refs. 3 and 4).

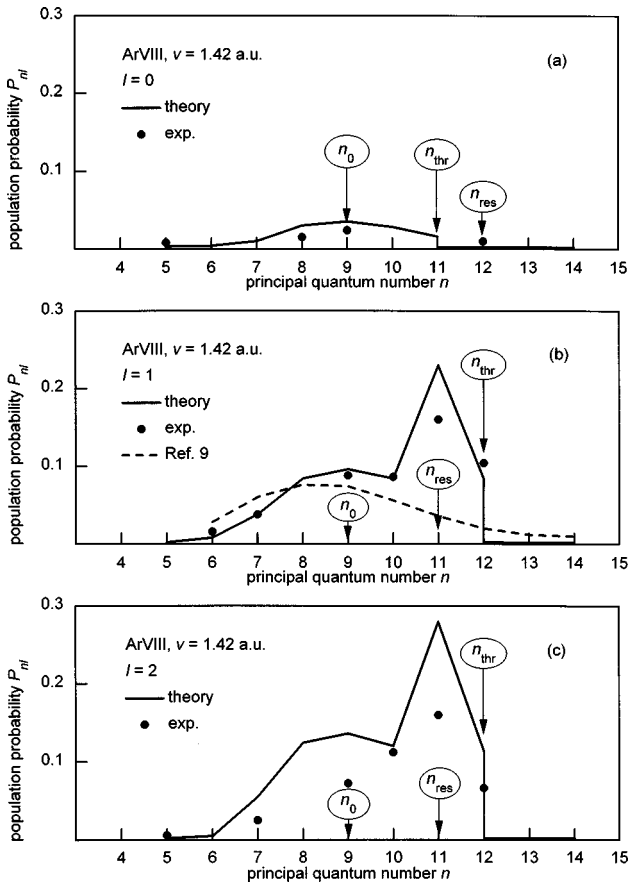

FIG. 7. Population probabilities P_{nl} of the Rydberg states (n,l) for Ar VIII ion ($v=1.42$ a.u.) with $l=0$, 1, and 2, respectively. Dots are experimental data (Ref. 2).

Fig. 6(b) follows the full line predicted by the present theory for $n<n_{\mathrm{thr}}$ (the same also holds for $l=0$ and 2).

In Fig. 7 we showed the population curves of Ar VIII ions with $E=2$ MeV ($v=1.42$ a.u.) taken from experiments.[2] Note the different P_{nl} scales in Figs. 5, 6, and 7. In the P_{nl} curves of Ar VIII with $l=1$ and 2, Figs. 7(b) and 7(c), very pronounced resonance shapes positioned at $n_{\mathrm{res}}=11$ are dominant. Obviously, these observable Ar VIII resonances arise with inverted positions of n_{thr} and n_{res} on the n scale (i.e., for $l=1$ and 2 we have $n_{\mathrm{res}}<n_{\mathrm{thr}}$). In Fig. 7(b) we marked the dashed JWKB curve, illustrating a limitation of our previous model[9] (in the region $n\approx n_{\mathrm{res}}=11$) as well as its correctness around the ''ordinary'' P_{nl} maximum placed at $n_0\approx Z$.

V. CONCLUDING REMARKS

The study explicated in this paper indicates that the selective low l Rydberg-state formation of multiply charged ions escaping a solid surface at intermediate velocities represents, essentially, a complicated quantum-mechanical event. At first sight, this complexity appears somewhat unexpected, because even the simple energetic arguments[1–4] (suggested at the very beginning of the experimental investigation of the process) tell us that the foil valence band is nearly resonant with the Rydberg states $n\sim Z$ of the multiply charged ions $Z=6$, 7, and 8.

All simple arguments fail, however, when we pass to a more detailed, ''fine-structure'' analysis of the P_{nl} curves, especially in the region $n>n_0\approx Z$. As we have seen, both resonances and thresholds appear in that region as the main structures in the shapes of the P_{nl} graphs. Moreover, a specific interplay of these two effects is characteristic of the considered ion-surface interaction. For this reason, it was not possible to treat separately the electron-capture process and the ionization of those Rydberg states formed dominantly above E_F. The mentioned charge-exchange processes are realized mainly in the vicinity of the potential barrier top, so that the ion-surface system is subjected to a kind of ''critical'' physical condition. This circumstance led us to the fact that even small changes in the parameters of the system (n, l, Z, or v) have resulted in drastic modifications of the P_{nl} curves for $n>n_0\approx Z$. The relative stability of the P_{nl} shapes established for $n\leqslant n_0\approx Z$ comes as a natural consequence of the validity of the deep underbarrier tunneling approximation.

A few additional concluding remarks may be relevant for further investigation of resonances and thresholds recognized in the P_{nl} curves of low l Rydberg-state formation.

First, it has been assumed in the matching procedure of the applied etalon equation method (Sec. III B) that the turning points $\tilde{\eta}_1$ and $\tilde{\eta}_2$ are sufficiently distant even in the case of tunneling in the very vicinity of the potential barrier top. This assumption appears as a correct one whenever the

Rydberg-state population process takes place dominantly at the critical ion-surface distance R_c. However, to have a more refined study of the role of the potential barrier top, it would be relevant to elucidate a process of the turning points confluence. In that case, an etalon equation method of the Kolosov type [see, e.g., Ref. 19, Chap. 2] will be a more adequate one. Including the confluence effect in our mixed flux dynamics, we expect that the shapes of Ar VIII resonance peaks characterizing the P_{nl} curves can be improved.

Second, the problem of intermediate Rydberg states formed dominantly above the Fermi level E_F was not discussed in more detail in this paper. In our model, the fast ionization condition (2.9) appeared to be sufficient to explain all observable facts of the existing experimental data, which has been the main intention of this paper. In that sense, only a brief review of the calculations is presented (Sec. III D). However, from a theoretical point of view, an additional investigation of the ion-surface interaction dynamics during the intermediate stages of time evolution of the process will be relevant. We point out here that the study of the quantity $\Gamma_{\mu}^{\mathrm{ion}}$ will differ in comparison to some still known asymptotic methods applied on the level of energy eigenvalue problem calculations.[20,21] The main difference lies in our parametrization of the eigenproblem by means of the scaling parameter α, combined with the etalon equation approach. Details of $\Gamma_{\mu}^{\mathrm{ion}}$ calculations, as well as a more complete dynamics (leading to more detailed P_{nl} curves for $n>n_{\mathrm{thr}}$), will be presented in our subsequent publications on the subject.

Third, considering the transition probability T_{nl}^{γ} (Sec. IV C), we recognized the quasiresonant kernels $\gamma_{\max} \rightarrow \gamma_A(R_c)$ of underbarrier type as the dominant transition ''directions'' from the solid valence band into the considered Rydberg states (n,l). The nonresonant electron-capture ''directions'' $\gamma \rightarrow \gamma_A(R_c)$, satisfying the condition $\gamma < \gamma_{\max}$ or $\gamma > \gamma_{\max}$, are taken into account in our calculation of the total transition probability T_{nl}. Strictly speaking, this approach is based on a validity of the T_{nl}^{γ} expression extended from the vicinity of the point $(\gamma_{\max}, t_c)$ over the entire γt plane. For the ionic parameters tested in this paper, this approximation cannot change the T_{nl} probability significantly because we obtain sufficiently pronounced maxima for both T_{nl}^{γ} and $\tilde{\Gamma}_{nl}^{\gamma}$, especially in the case of Ar VIII resonances. A more precise analysis can be given by a refined classification of the Φ_{MA} components in the mixed flux I_{nl}^{γ}, including the overbarrier Φ_{MA} eigenfunctions as possible contributions for $\gamma < \gamma_{\max}$. To resolve this problem, it is necessary to extend the etalon equation method in the complex $\tilde{\eta}$ plane, after which an appropriate quantum dynamics must be developed.

Finally, in presenting our numerical results, we used the value $\phi = 3$ eV for the work function of the carbon foil (Secs. IV B and IV D). We realized that this choice is fitting to the available experimental data. However, according to our dynamic model, the positions of resonances and thresholds in the P_{nl} curves are dependent on the work function ϕ, so that the observable P_{nl} curves could differ greatly with different values of ϕ. Accordingly, various surface contamination effects (resulting in the change of ϕ) can influence to a high degree the experimentally obtained P_{nl} curves, especially in the higher n region. The problem of the ϕ instability requires further work in both theory and experiment.

A general observation about Demkov-Ostrovskii's methodology, applied in this paper, could be of use. Bearing in mind that this method[10] was originally developed for arbitrary projectile velocities of ion-atom collisions, it can be used not only as a basis in the investigation of the resonances and thresholds at $v \sim 1$ a.u., but also in a study of the adiabatic limit ($v \ll 1$ a.u.) of the electron capture into Rydberg states of multiply charged ions escaping the solid surface. Our preliminary calculations indicate that, from the standpoint of quantum dynamics based on the mixed flux, the limiting v procedure represents a rather subtle mathematical problem, strongly dependent on the values of the ionic parameters n, l, m, and Z. We found that the expected resonant nature of the electron capture appears as a consequence of the limiting procedure.

Some of the known results,[5–8] relevant in the case of low velocity, can be recognized as an output of our analysis. For example, under the adiabatic conditions, it emerges a challenging universality[7,8] of the differential transition rate $d\Gamma/(2\gamma d\gamma)$, which represents a function exclusively dependent on the scaling parameter α. Also, considering the mentioned transition rate as a function of R, we obtain that the Rydberg-state formation of a multiply charged ion is dominantly localized around the critical ion-surface distances R_c. A remarkable distortion of the electron cloud (in comparison to the free atomic state) is found at distances $R < R_c/2$. In this region of the ionic trajectory, we realized that the electron density distributions are dependent on the form of the surface potential.

[1] B. Andreson, B. Denne, J. O. Ekberg, L. Engstrom, S. Huldt, I. Martinson, and E. Veje, Phys. Rev. A **23**, 479 (1981).

[2] S. Bashkin, H. Oona, and E. Veje, Phys. Rev. A **25**, 417 (1982).

[3] E. Veje, Nucl. Instrum. Methods Phys. Res. B **9**, 586 (1985).

[4] E. Veje and H. Winter, Z. Phys. D **10**, 457 (1988).

[5] J. Burgdörfer, in *Review of Fundamental Processes and Applications of Atoms and Molecules*, edited by C. D. Lin (World Scientific, Singapore, 1993), p. 517.

[6] U. Wille, Phys. Rev. B **50**, 1888 (1994).

[7] P. Nordlander, Surf. Sci. **388**, L875 (1995).

[8] P. Kürpick and U. Thumm, Phys. Rev. A **54**, 1487 (1996).

[9] N. N. Nedeljković, Lj. D. Nedeljković, S. B. Vojvodić, and M. A. Mirković, Phys. Rev. B **49**, 5621 (1994).

[10] Yu. N. Demkov and V. N. Ostrovskii, Zh. Eksp. Teor. Fiz. **69**, 1582 (1975) [Sov. Phys. JETP **42**, 806 (1976)].

[11] N. N. Nedeljković, Lj. D. Nedeljković, R. K. Janev, and Z. L. Mišković, Nucl. Instrum. Methods Phys. Res. B **58**, 519 (1991).

[12] S. Bashkin, E. Träbert, P. H. Heckmann, H. v. Buttlar, and K. Brand, Phys. Scr. **28**, 193 (1983).

[13] S. Yu. Slavyanov, Diff. Eqs. **5**, 313 (1969) (in Russian).

[14] S. Yu. Slavyanov, in *Problems in Mathematical Physics*, edited

by M. S. Birman (Leningrad State University, Leningrad, 1970), Vol. 4, p. 125 (in Russian).
[15] L. D. Landau and E. M. Lifshitz, *Quantum Mechanics* (Nauka, Moscow, 1989), p. 646 (in Russian).
[16] H. Buchholz, *The Confluent Hypergeometric Functions* (Springer, Berlin, 1969), Sec. 8.1, p. 101.
[17] M. Abramovitz and I. Stegun, *Handbook of Mathematical Functions* (Dover, New York, 1972), pp. 448 and 508.
[18] A. Messiah, *Quantum Mechanics* (North-Holland, Amsterdam, 1970), Vol. I, p. 110.
[19] *Rydberg States of Atoms and Molecules*, edited by R. F. Stebings and F. B. Dunning (Cambridge University Press, New York, 1983).
[20] A. V. Chaplik, Zh. Eksp. Teor. Phys. **54**, 332 (1968) [Sov. Phys. JETP **27**, 178 (1968)].
[21] N. N. Nedeljković, Fizika (Zagreb) **18**, 275 (1980).